JOURNAL OF CATALYSIS **168,** 278–291 (1997)
ARTICLE NO. CA971625

Characterization of Activated States of Ruthenium-Containing Zeolite NaHY

Shie-Ping Sheu,[1] Hellmut G. Karge,[2] and Robert Schlögl

Fritz Haber Institute of the Max Planck Society, Faradayweg 4-6, 14195 Berlin, Germany

Received November 1, 1995; revised January 17, 1997; accepted January 24, 1997

As has been proven earlier, ruthenium-containing NaHY zeolites are able to catalyze the decomposition of ammonia at temperatures from 300 to 450°C. In such catalysts, ruthenium cations are still present, even after heat treatment in high vacuum at 400°C; they can be detected using ammonia and/or pyridine as probes for Fourier transform IR spectroscopy. They reside both in supercages and in sodalite cages. Various intermediates of the decomposition of the $Ru(NH_3)_6NaY$ complex on heat treatment in high vacuum were identified via *in situ* IR spectroscopy; in particular, evidence for the formation of complexes with nitrosyl ligands was obtained. It was shown that partially decomposed (deammoniated) $Ru(NH_3)_6NaY$ complexes can be recovered to some extent by readsorption of ammonia. Ruthenium-containing species were localized either in the supercages or in the small cavities as shown by IR spectroscopy employing ammonia and pyridine as probes. The acidic properties of variously treated $Ru(NH_3)_6NaY$ zeolites were characterized via temperature-programmed desorption (TPD) of ammonia, which was monitored by mass spectrometry. A strong interaction between ruthenium-containing species and the zeolite framework, leading to a lack of overtone and combination modes in the near infrared, is confirmed. Investigations of $Ru(NH_3)_6NaY$ samples by X-ray photoelectron spectroscopy under the same conditions as applied for IR and TPD studies revealed that, at variance with the results usually obtained after heat treatment of $Ru(NH_3)_6NaY$ in high vacuum, no significant formation of ruthenium metal species through autoreduction occurred. Rather, a particular form of a cation-exchanged Ru, Na-Y zeolite was obtained.

INTRODUCTION

Ruthenium has recently received considerable attention in the field of improved catalysts for ammonia synthesis (1), in competition with traditional iron catalysts. Ruthenium-exchanged zeolite NaY was also found to be an active catalyst in ammonia synthesis (2–4). The activity of ruthenium metal particles inside the cavities of faujasite-type zeolites was reported to be dependent on the type of cation present in the zeolite, the silicon-to-aluminum ratio, and the size of the metal particles (4). So far, these works have shown promising catalytic applications for ruthenium-containing zeolite NaY; however, the materials have been characterized mostly by methods other than IR spectroscopy, e.g., X-ray photoelectron spectroscopy (XPS), X-ray diffraction (XRD), transmission electron microscopy (TEM). The aim of the present study was to investigate the acid sites, the activated states, and the distribution of ruthenium-containing species in view of the catalytic properties of the ruthenium-containing Y zeolite. Combinations of NH_3 and pyridine probing techniques were used that should provide valuable information about the activated states of the zeolite. Fourier transform IR (FTIR) spectroscopy, temperature-programmed desorption monitored by mass spectrometry (TPD–MS) and XPS were employed.

EXPERIMENTAL

NH_4Y zeolite was obtained from NaY (Degussa) by 10-fold exchange with 0.1 *M* ammonium chloride solution at 70°C. To remove residual salt, the exchanged sample was washed with distilled water until it was free from Cl^- ions as indicated by adding $AgNO_3$ solution. The ruthenium complex was exchanged into the NaY zeolite at room temperature for 24 h by using $[Ru(NH_3)_6]Cl_3$. The product was dried at ambient temperature and eventually turned deep purple. The materials used had the following compositions (according to bulk elemental analysis): NaY, $Na_{56}[(AlO_2)_{56}(SiO_2)_{136}]$; NH_4Y, $(NH_4)_{56}[(AlO_2)_{56} \cdot (SiO_2)_{136}]$; $Ru[(NH_3)_6]NaY$, $Ru_9Na_{29}[(AlO_2)_{56}(SiO_2)_{136}]$.

The *in situ* spectra in the mid-IR region were obtained on a Perkin–Elmer 2000 FTIR spectrometer and were run in the transmission mode with self-supporting wafers having a "thickness" of about 7 mg cm^{-2}. The infrared cell was sealed with CaF_2 windows by Viton O-rings. This quartz infrared cell was designed to permit *in situ* spectrum recording during heating or gas adsorption, and was connected to an ultrahigh vacuum system (5, 6). The gas dosing was monitored with a Baratron manometer (Model 220, BHS, from MKS Co., München, Germany) and a needle valve.

[1] On leave from the Department of Chemistry, National Tsing Hua University, Hsinchu, Taiwan.

[2] To whom correspondence should be addressed.

0021-9517/97 $25.00

Pyridine was supplied by Merck, Darmstadt, Germany, purified by three freeze–pump–thaw cycles, and subsequently dried over activated Linde 3A sieve; ammonia from Messer Griesheim, Düsseldorf, Germany, was used without further purification.

The near-infrared spectra were recorded by diffuse reflectance (DRIFTS) on the same Perkin–Elmer 2000 FTIR spectrometer at a resolution of 4 cm^{-1} with about 200 scans. Aluminum foil was used as a reference. The device used for the investigations by DRIFTS was homemade. The description and further experimental details are provided elsewhere (7).

Temperature-programmed desorption of adsorbed species was carried out in an ultrahigh vacuum system equipped with a mass spectrometer (Balzers QMG 311, Nordenstadt, Germany) (8). All the zeolite samples studied were pressed into wafers of 10 mg cm^{-2}.

For XPS, the starting material was deposited from an aqueous slurry onto a gold single crystal. This sample was fixed to a variable-temperature holder, which could be operated in UHV or under atmospheric pressure of hydrogen. Spectra were taken with a modified Leybold EA 200 analyzer in the pass energy mode with a resolution of 1.1 eV and Mg$K\alpha$ excitation at 200 W. The sample charging was corrected using the Al 2*s* level at 117.5 eV as an internal standard. This value gave the common binding energies for silicon, oxygen and carbon, which were checked with the Na-Y precursor zeolite.

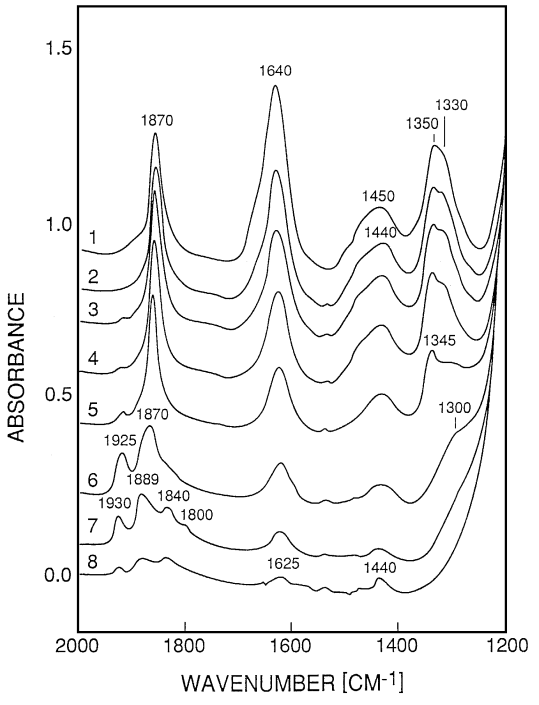

FIG. 1. *In situ* IR spectra of $Ru(NH_3)_6NaY$ on deammoniation by heat treatment in high vacuum at 25 (1), 50 (2), 75 (3), 100 (4), 150 (5), 200 (6), 250 (7), and 300°C (8); region of deformation vibrations.

RESULTS AND DISCUSSION

1. Deammoniation

It has been established that $Ru(NH_3)_6^{3+}$ exchanged into the supercages of Y zeolite will hydrolyze with zeolite-sorbed water and become partially oxidized to form $[Ru(NH_3)_5OH]^{2+}$ or $[(NH_3)_5RuORu(NH_3)_4O \cdot Ru(NH_3)_5]^{6+}$, Ru-red, or will undergo decomposition when the sample is exposed to air (9–11). The *in situ* IR spectra of samples deammoniated at various temperatures are shown in Figs. 1 and 2. The samples were deammoniated at a heating rate of 5°C min^{-1} and the spectra were recorded at different temperatures. After preevacuation at 25°C, the spectrum (Fig. 1.1) reveals the presence of four bands at 1870, 1640, 1450, and 1350 cm^{-1}; a shoulder at 1330 cm^{-1} was also observable. The change in the coordination sphere of the ligands on raising the temperature was confirmed by the frequency shift of the band of coordinated NH_3 (1350–1345 cm^{-1}). The symmetry of the ruthenium hexammine complex was altered as a consequence of the partial removal of coordinated NH_3 ligands. This change in the coordination symmetry was also evidenced by Goldwasser *et al.* with the electron spin resonance (ESR) technique (12). They reported that the crystal field symmetry around Ru^{3+} decreased from tetragonally distorted octahedral to orthorhombic in the case of outgassing at room temperature.

The band at 1640 cm^{-1} became narrower after room temperature evacuation. This band is attributed to the deformation vibration mode of adsorbed H_2O that was originally trapped in the zeolite. At lower temperatures it overlaps with the band due to coordinatively bound NH_3 at around 1620 cm^{-1}. The IR spectra of water molecules, which formed hydrogen bonds with H^+ in the zeolite cages, exhibit a broad band in the range 2800 to 3500 cm^{-1}. Thus, H_2O prevents the observation of NH stretching bands within this region at low temperatures. The band at 1870 cm^{-1} was in the typical range of coordinated nitrosyl ligands and indicated the formation of $[Ru(NH_3)_5(NO)]^{3+}$ in the supercages of zeolite Y. Under our experimental conditions, the oxygen atom of the NO ligand may originate from the water molecules previously existing inside the cages of the zeolite.

During the decomposition of $Ru(NH_3)_6NaY$ zeolite at elevated temperatures, a variety of intermediates were observed. At 200°C, a new band at 1925 cm^{-1} gradually formed coupled with a further frequency shift of the band due to coordinated NH_3 to 1300 cm^{-1}. In fact, the presence of additional ligands on the metal can influence the bonding between the metal and the nitrosyl group. Thus, electropositive ligands will reduce the ability of the metal

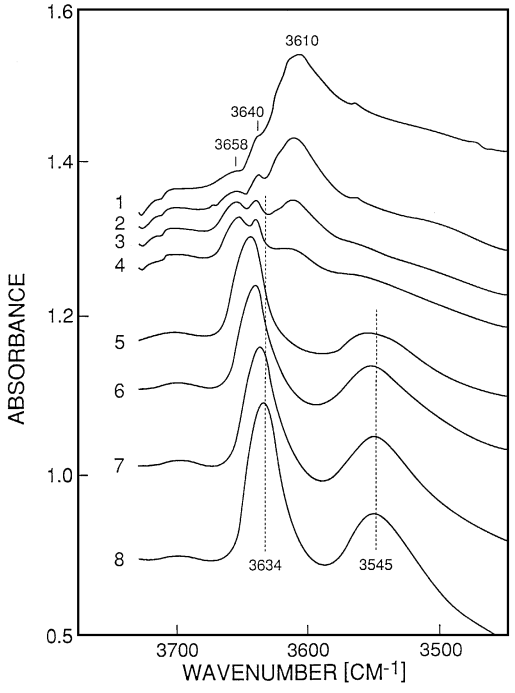

FIG. 2. *In situ* IR spectra of $Ru(NH_3)_6NaY$ on deammoniation by heat treatment in high vacuum at 25 (1), 50 (2), 75 (3), 100 (4), 150 (5), 200 (6), 250 (7), and 300°C (8); region of stretching vibrations.

to provide *d* electrons for $2\pi^*$ backbonding, which will, hence, result in a weakening of the metal–ligand bond and a strengthening of the N–O bond. Therefore, the band at 1925 cm^{-1} could arise from several different ruthenium–nitrosyl complexes such as $[Ru(NH_3)_4(NO)(OH_2)]^{3+}$ and $[Ru(NH_3)_4(NO)(OH)]^{2+}$ in which the counterligands, NH_3, H_2O, and OH, might possibly form hydrogen bonds with framework protons or be in contact with Na^+ cations. Evacuation at 250°C gave more types of nitrosyl species as indicated by bands at higher frequencies of 1930 and 1890 cm^{-1} and at lower frequencies of 1840 and 1800 cm^{-1}. The generation of these lower-frequency NO bands, i.e., at 1840 and 1800 cm^{-1}, indicated that the counterligands had a more electronegative character. When outgassing above 100°C, the formation of complexes such as $[Ru(NO)(NH_3)_{1,2}(O_z, OH, H_2O)_{4,3}]^{3+}$ may occur. That is, at this temperature, the ruthenium atom might be attached to the zeolite wall and bound to the framework oxygen atoms (O_z), which might account for these bands. An alternative explanation would be that the ligand OH (without hydrogen bonding or cation influence) lowers the nitrosyl stretching frequency, and simultaneously, the oxidation state of Ru decreases from (+3) to (+2). The increase in $\tilde{\nu}(NO)$ to values above 1900 cm^{-1} might then be due to incorporation of NO_2 ligands, which could form on oxidation of NO (13). At temperatures higher than 300°C, the IR spectrum no longer showed ligand bands, and this suggested that most, if not all, of the ligands could be removed by evacuation above 300°C. Hereafter, the deammoniated $Ru(NH_3)_6NaY$ material is denoted as Ru/NaHY, which should be taken to indicate that it also contains OH groups (see later).

On preevacuation of the zeolite at 25°C, a broad absorption in the range from about 2800 to 3500 cm^{-1} and three distinct bands at 3610, 3640, and 3658 cm^{-1} were observed (Fig. 2). The band at 3658 cm^{-1} is usually ascribed to OH groups attached to extraframework cationic species.

On outgassing at higher temperatures, bands at 3634 and 3545 cm^{-1} gradually appeared and became well resolved above 300°C. It is generally accepted that the OH stretching vibrations are due to high-frequency (HF) hydroxyl groups, located in the supercages, and low-frequency (LF) hydroxyl groups in the sodalite cages, generated by proton attachment to the zeolite Y framework according to the Hirschler–Plank mechanism (14, 15). Both the OH (HF) and OH (LF) bands of Ru/NaHY shifted to lower frequencies in comparison with those in HY zeolite, viz., 3640 and 3550 cm^{-1}. This may imply that the O–H bond was modified by the presence of ruthenium species. The band areas of OH (HF) and OH (LF) in highly exchanged HY zeolites were 36 and 64%, respectively. If one assumes that the extinction coefficients of both OH (HF) and OH (LF) bands on HY and Ru/NaHY were comparable, the OH groups, generated via the ion-exchange process, were estimated to be equal in number on both OH (HF) and OH (LF) sites and in total about 45% of those in HY zeolite. Only a small band at 3740 cm^{-1} of terminal SiOH could be detected and was not affected by the deammoniation process. Moreover, a fraction of the OH (HF) and OH (LF) groups may have formed via NH_3 ligand replacement by interaction with residual H_2O (hydrolysis). This would result in the formation of OH ligands and exchange of Na^+ by NH_4^+, giving rise to OH groups of the framework on deammoniation.

2. *Ammonia Readsorption*

After pretreatment at 300°C, most of the ruthenium was located inside the cages of the zeolite Y (see Fig. 3). It is very likely that the acid strength and distribution of OH groups will be altered by the presence of ruthenium species and thus differ from those in the HY zeolite. By ammonia readsorption some valuable information could be obtained. The reaction of the OH groups with ammonia molecules and their recovery was monitored by IR. To rule out any factors that would cause additional differences between the spectra e.g., changes in the position of the wafer which would cause a background difference, *in situ* sample activation and direct spectrum recording were performed. The wafer was first deammoniated at 400°C for 2 h and then exposed to ammonia at 25°C. For the $Ru(NH_3)_6NaY$ zeolite, a second experiment with an additional reduction treatment was performed for the purpose of comparison. The IR spectra obtained after evacuation at 25°C were used as a reference spectrum, and all the spectra in Fig. 4 were plotted as difference

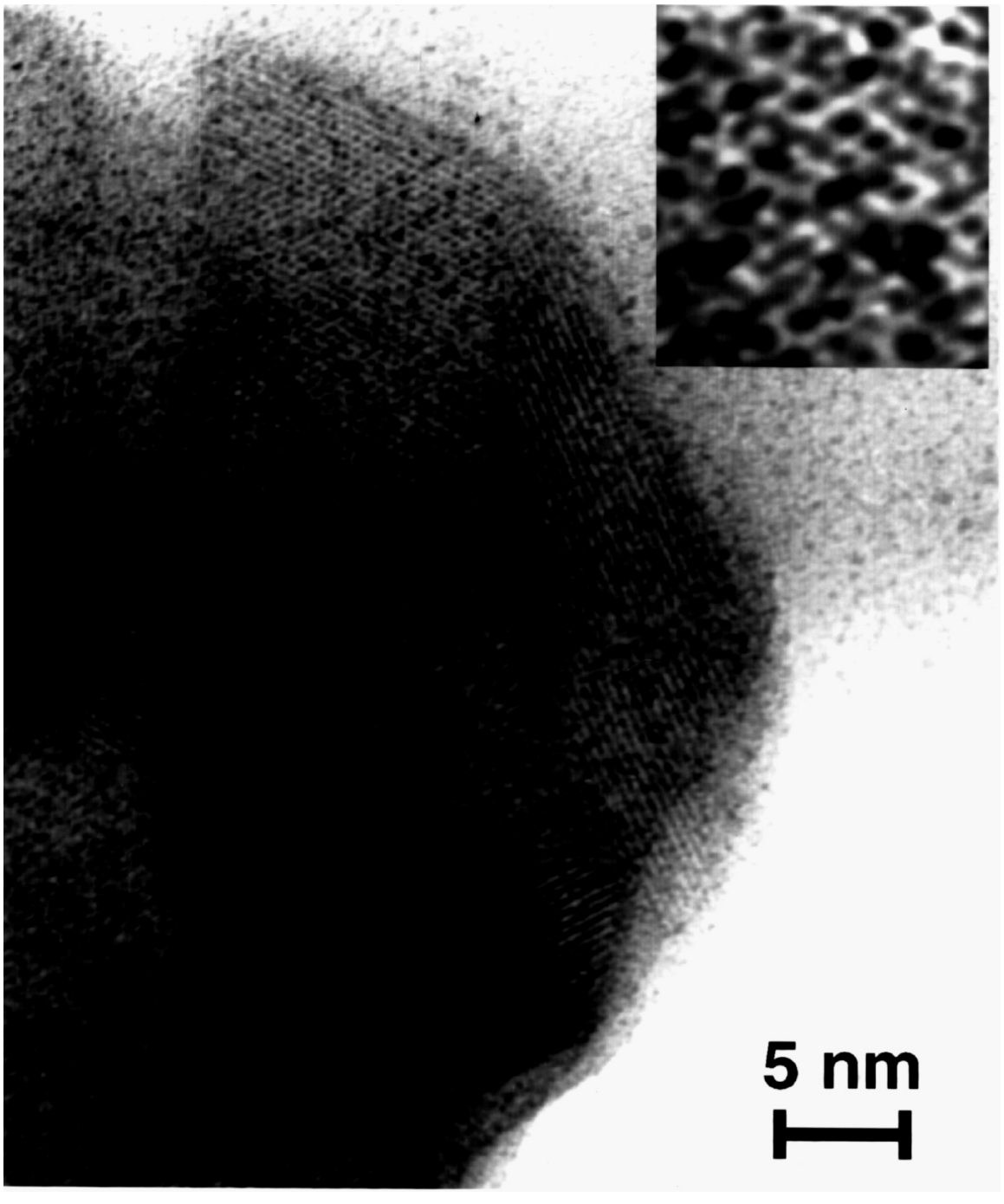

FIG. 3. Transmission electron micrograph of an autoreduced $Ru(NH_3)_6NaY$ sample. Autoreduction occurred on heating the $Ru(NH_3)_6NaY$ wafer at a rate of 5°C min^{-1} to 400°C and treatment at 400°C in high vacuum ($<10^{-5}$ mbar) for 12 h. The average particle size is 1 to 1.5 nm.

spectra with respect to these references. The maximum and equilibrium adsorption of ammonia was determined by a series of dosings until no further increase in intensity of the NH_4^+ bands was observed, and complete reaction of the OH bands with ammonia molecules had occurred.

It can be seen from Figs. 4b and c that the IR spectra of ammonia readsorbed on the Ru/NaHY after additional reduction treatment and on HY zeolites were similar. They differed in the numbers of dosings necessary to reach saturation, viz., 5 and 10 for Ru/NaHY and HY, respectively. Since the wafers were pressed to identical thickness (5 mg/cm^2) and size (1 × 2 cm^2), the relative amount of consumed ammonia may indicate the relative numbers of acid sites in each sample. From this semiquantitative titration,

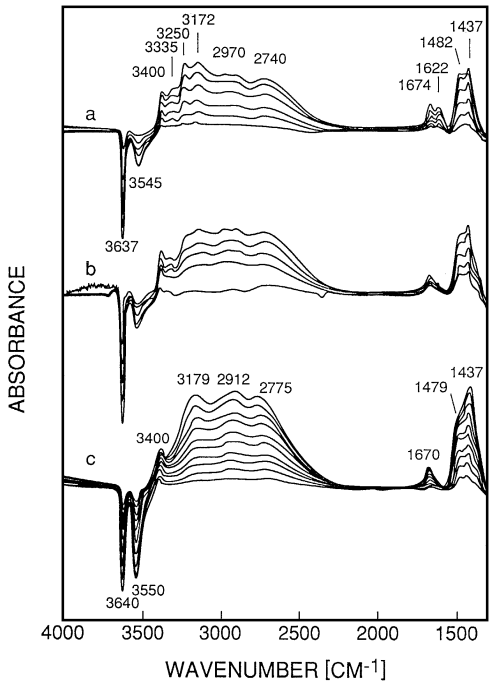

FIG. 4. IR difference spectra of Ru/NaHY and HY after readsorption of increasing amounts of NH_3 onto (a) Ru/NaHY (activated at 400°C in HV), (b) Ru/NaHY (activated at 400°C and subsequently reduced at 400°C and 266 mbar H_2), and (c) HY (activated at 400°C in HV).

the number of OH groups in the Ru/NaHY zeolite was estimated to be about half of that in the HY zeolite, in agreement with the previous estimation from the OH band area.

The IR spectra of ammonia interacting with protons of HY exhibited NH stretching bands at 3400, 3179, 2912, and 2775 cm^{-1} as well as bending bands at 1670, 1479, and 1437 cm^{-1}. When an excess of ammonia was dosed into the system, the last two bending bands usually merged to give, in HY zeolite, a broad band with a maximum at 1445 cm^{-1}. However, it can be clearly seen in Fig. 4a that an additional set of IR bands, viz., at 3335, 3250, 2740, and 1622 cm^{-1}, were detected on ammonia readsorption on Ru/NaHY zeolite that was subjected only to heating in high vacuum (see later). The assignments of the bands observed are as follows. According to the literature (16, 17), the spectral characteristics of ammonia or ammonium ions are as shown in Table 1.

TABLE 1

Assignment of IR Bands[a] of NH_3 and NH_4^+

Compound	$\nu_1(\nu_s)$	$\nu_2(\delta_s)$	$\nu_3(\nu_{as})$	$\nu_4(\delta_{as})$
NH_3 (gas)	3336	968–932	3444	1628
NH_3 (solid)	3223	1060	3378	1646
NH_4^+	3040	1400	3154	1680

[a] All data in cm^{-1}.

The bands at around 1440 cm^{-1} can be assigned to δ_s (symmetric deformation vibration), and the band at 1670 cm^{-1} is due to δ_{as} (asymmetric deformation vibration) of NH_4^+ originating from ammonia bonded to Brønsted acid sites, whereas for the Ru/NaHY zeolite without reduction, the additional band at 1622 cm^{-1} might be the asymmetric deformation vibrational band of NH_3 bonded to Lewis acids or other cations. The NH_3 is not strongly adsorbed on ruthenium metal because there is no empty *d* orbital to accommodate the lone-pair electrons from the N atom. Therefore, the band at 1622 cm^{-1} is thought to be due to NH_3 associated with residual ruthenium cations, i.e., NH_3–Ru^{n+}, which also holds for the bands at 3335 and 3250 cm^{-1} (see later). The above assignment of these three bands was also suggested by the observation that they did not reappear in the IR spectrum after NH_3 readsorption when the sample was further subjected to reduction treatment (Fig. 4b). Since the control of complete reduction of ruthenium cations is important with respect to the catalytic application of Ru/NaHY, the ammonia probing technique could be a useful method to characterize the ruthenium-containing catalyst. As described in the next section, we found, by a combination of ammonia and pyridine adsorption, that indeed a fraction of the residual ruthenium cations probed by ammonia were located inside the sodalite cages.

When evacuated only below 300°C, many of the ruthenium complexes were not fully decomposed and were presumed to be able to undergo ligand replacement. Figure 5 shows the IR spectra of ammonia readsorption (solid lines) on the samples that were previously deammoniated at 100, 150, 200, 250, and 300°C. For comparison, the dashed lines in Fig. 5 represent the spectra of the samples deammoniated at the indicated temperatures. The ammonia readsorption on samples that were pretreated at lower temperatures showed interesting phenomena. First, the 1270 cm^{-1} band intensity, which was due to coordinatively bound ammonia of lower ligand symmetry, decreased, and the 1320 cm^{-1} band intensity, which was indicative of coordinatively bound ammonia of higher ligand symmetry, increased. This implies that NH_3 molecules can replace part of the nonammonia ligands in the ruthenium complex. Second, all the band intensities from NO species (2000–1800 cm^{-1}), which were generated by deammoniation at 100, 150, or 200°C, decreased or even completely disappeared. This suggests that the NO ligands could be replaced by NH_3 molecules and the ruthenium ammine complex could thus be regenerated to some extent. Third, if the sample was pretreated in high vacuum at 300°C, ruthenium cations, Ru^{n+}, still remained inside the zeolite Y cavities as evidenced by the 1625 cm^{-1} band.

The desorption of adsorbed ammonia is frequently used as a method to discriminate the strength of interaction of different sites. As we already found, there are at least two types of acidic sites, namely, protons and ruthenium cations, that occur in the Ru/NaHY zeolite. Therefore, the ammonia

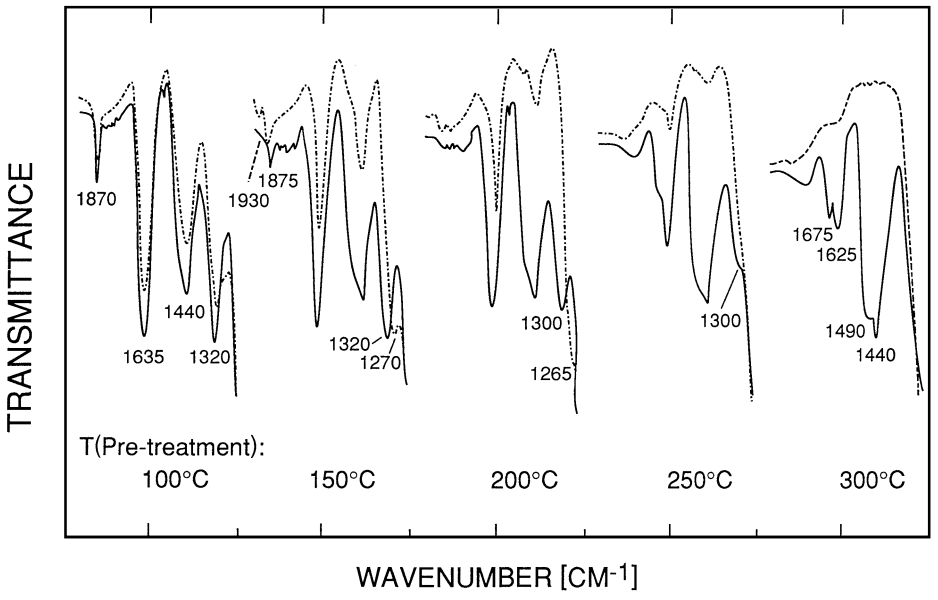

FIG. 5. IR spectra of $Ru(NH_3)_6NaY$ heat-treated at increasing temperatures and reloaded with ammonia. Dashed lines: prior to NH_3 readsorption; solid lines: after readsorption of NH_3.

desorption after readsorption of ammonia on Ru/NaHY and HY zeolites was further monitored by *in situ* IR spectroscopy. After reloading with ammonia, the wafer was first evacuated at room temperature for 0.5 h, and subsequently *in situ* IR spectra were recorded during heating from 25 to 320°C at a heating rate of 5°C min^{-1} for each sample. Figure 6 shows five to six selected *in situ* IR spectra of NH_3 desorption from NH_3-loaded Ru/NaHY and HY zeolites. Again, all of the spectra in Fig. 6 were plotted as difference spectra with respect to the IR spectra obtained after degassing at 30°C. The calculated absorbances of the OH bands were plotted as a function of the evacuation temperature and are shown in Fig. 7. From the system NH_3–HY zeolite (Fig. 7b), more NH_3 associated with OH (LF) acid sites desorbed already at lower temperatures, probably due to the local structural environment of the respective acid sites.

In contrast to NH_3–HY, the OH (HF) groups of Ru/NaHY (Fig. 6a) appeared first, followed by the OH (LF). An explanation for this observation could be that a number of the ruthenium-containing species were in the sodalite cages and sited near the OH (LF) groups. This may strengthen the interaction between the ammonia molecules and the Brønsted sites inside the sodalite cage. In fact, earlier results from XRD have shown that ruthenium-containing species exist not only in supercages but also in sodalite cages (18), and they probably affect the OH group properties in Ru/NaHY zeolite by either through-space or through-lattice oxygen interaction. In the case of NH_3–Ru/NaHY, it is obvious that the NH_3–Ru^{n+} bands at 1622 cm^{-1} (see Fig. 6) disappeared at higher temperatures than did the bands around 1450 cm^{-1} originating from NH_3 interacting with Brønsted acid sites. The bands at 3335 and 3250 cm^{-1} exhibited similar behavior. Thus, these three bands (at 1622, 3335, and 3250 cm^{-1}) were ascribed to a second set of adsorbed ammonia species, viz. to NH_3–Ru^{n+} species.

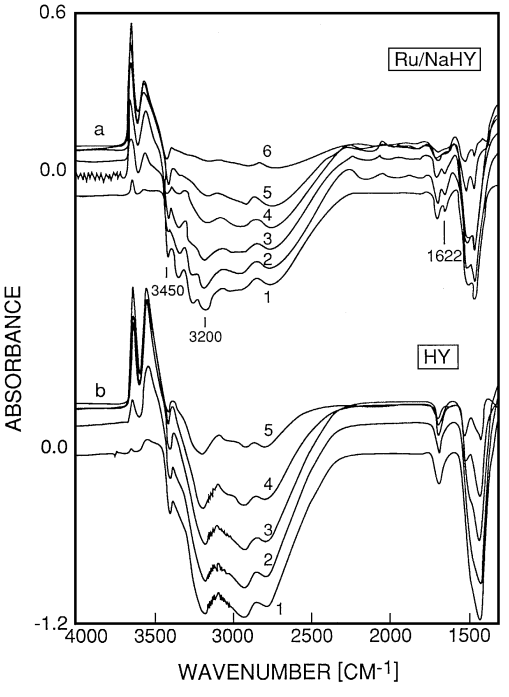

FIG. 6. IR difference spectra of (a) Ru/NaHY and (b) HY after reloading with NH_3 and subsequent desorption at 90 (1), 150 (2), 210 (3), 250 (4), 290 (5), and 310°C (6).

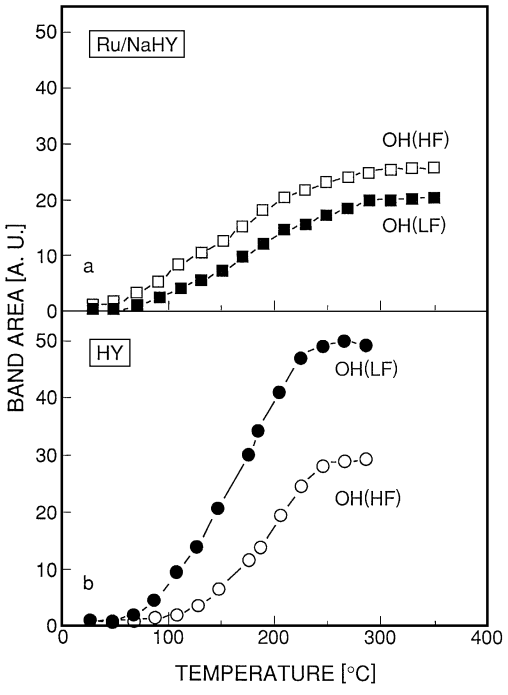

FIG. 7. Recovery of the OH bands of (a) Ru/HNaY and (b) HY after reloading with NH_3 and subsequent desorption at increasing temperatures.

3. Pyridine Adsorption

Pyridine adsorption has been proven to be a powerful tool for the characterization of acid sites in zeolites. Three infrared bands of the pyridine deformation mode in the range 1400–1650 cm^{-1} can be used to distinguish surface acid sites: (i) bands between 1430 and 1460 cm^{-1} provide information about Lewis acid sites which might be associated with pyridine attached to so-called true Lewis acid sites (Al-containing extraframework species), or pyridine coordinatively bonded to cations; (ii) bands in the region 1540–1550 cm^{-1} are due to pyridinium (PyH^+) ions formed on the consumption of Brønsted acidity; (iii) the contribution of both Lewis and Brønsted acid sites show bands around 1490 cm^{-1}. Therefore, the acid sites in this ruthenium-containing Y zeolite could also be elucidated by the pyridine probing technique.

After activation at 300°C for 2 h, the Ru/NaHY zeolite was exposed to pyridine vapor at 100°C for 1 h. Subsequent outgassing at 100°C was performed to desorb weakly interacting pyridine molecules. Prior to the IR measurement, the wafer was cooled to room temperature, evacuated at room temperature, and then stepwise heated to 300°C for *in situ* IR investigation. The high-frequency region of the pyridine desorption experiments is shown in Fig. 8. Surprisingly, a very broad band formed at room temperature and covered the whole range of initial OH bands. In the case of HY, pyridine reacts with the OH (HF) groups and the corresponding IR band vanishes. The present observation with Ru/NaHY suggests a weaker interaction between OH (HF) groups and pyridine molecules. There is no evidence for a lower strength of the OH (HF) of Ru/NaHY compared with HY zeolite. Therefore, it seems more likely that a fraction of the OH (HF) groups in the Ru/NaHY sample are partially shielded by small ruthenium-containing particles inside the supercages. In other words, these OH (HF) groups in the Ru/NaHY zeolite were less accessible to pyridine molecules compared with those in HY zeolite. This causes a weaker interaction with the OH (HF) groups, which results in broadening instead of vanishing of the respective band.

On raising the temperature to 300°C, both types of OH groups partially recovered (Fig. 8), and the intensity of the 1546 cm^{-1} band decreased to some degree (see Fig. 9). The OH (LF) band appeared more quickly than the OH (HF) band. Obviously, the OH (LF) band was only overlapped by the band resulting from perturbed OH (HF) groups.

The IR spectra of the low-frequency region are shown in Fig. 9. A series of bands appeared in the range 1400 to 1700 cm^{-1}, i.e., at 1627, 1615–1605, 1590, 1546, 1490, and 1446 cm^{-1}. The band at 1627 cm^{-1} is due to an overlap of bands originating from pyridine attached to Brønsted and Lewis sites (1632 and 1620 cm^{-1}, mode 8a, 8b). When pyridine was adsorbed on activated NaY (not shown in the figures), more pronounced bands at 1595 and 1440 cm^{-1} were observed. Thus, the bands at 1590 and 1440 cm^{-1} were presumed to originate from pyridine coordinated to Na^+ cations. Since the Na^+ cations are weak acceptors and the

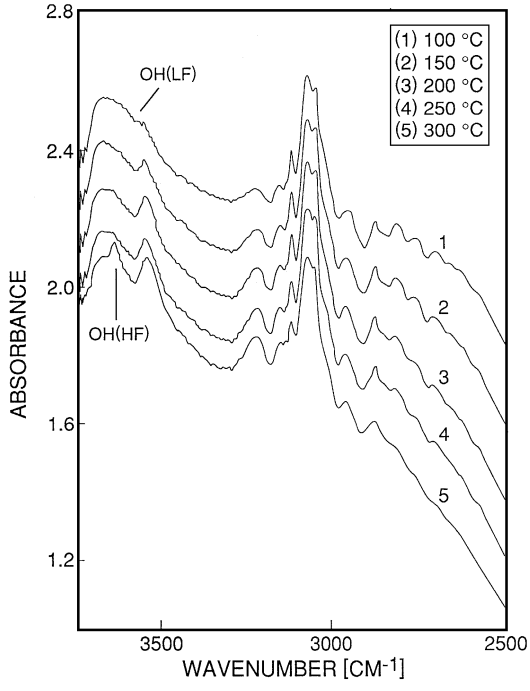

FIG. 8. *In situ* IR spectra of Ru/NaHY after pyridine adsorption at 100°C, predesorption at the same temperature, cooling to 35°C, and subsequent pyridine desorption at increasing temperatures; region of stretching vibrations.

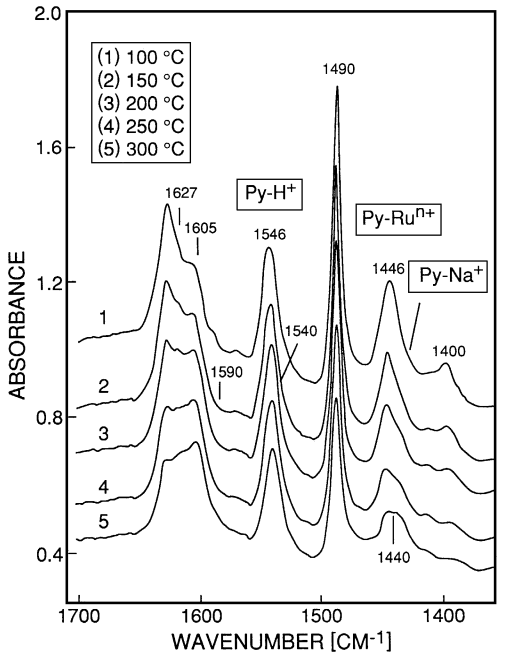

FIG. 9. *In situ* IR spectra of Ru/NaHY after activation at 300°C (high vacuum, 2 h), pyridine adsorption at 100°C, predesorption at the same temperature, cooling to 35°C, and subsequent pyridine desorption at increasing temperatures; region of deformation vibrations.

pyridine adsorbed on them was mostly removed by 100°C desorption pretreatment, the band intensity was relatively small in the case of Ru/NaHY.

The band at 1446 cm^{-1} exhibited stronger thermal stability and thus was ascribed to pyridine adsorbed on ruthenium cations, i.e., Py–Ru^{n+}. Since the ruthenium complex was shown to undergo ligand replacement below 300°C, more Py–Ru^{n+} species should be formed on exposure of the $Ru(NH_3)_6NaY$ zeolite to pyridine vapor at room temperature. Subsequent heating should enable the pyridine molecules to partially replace NH_3 ligands. This experiment was performed under 5 mbar pyridine pressure. The *in situ* IR spectra are shown in Fig. 10. It can be seen that at 30°C the bands associated with pyridine molecules only occurred at 1590, 1540, 1486, and 1440 cm^{-1}. The bands at 1590 and 1440 cm^{-1} represent the interaction of pyridine with Na^+ cations. The disappearance of the broad NH_4^+ band around 1450 cm^{-1} (compare, e.g., Fig. 1) together with the formation of the band at 1540 cm^{-1} confirmed that the pyridine molecules had interacted with framework OH groups at 30°C. The shapes of the bands due to NH_3, H_2O, and NO ligands were more or less perturbed but with no obvious decrease in intensity at 30°C. On a gradual increase in the temperature from 30 to 300°C, the Py–Ru^{n+} band at 1448 cm^{-1} was generated as expected. Thus, the assignment of this band was confirmed. By comparison of the intensity at 1448 cm^{-1} with that of PyH^+ at 1540 cm^{-1}, it is obvious that the amount of Py–Ru^{n+} species in this experiment was much larger than that in the experiment shown in Fig. 9, in which it is most likely that part of the ruthenium species was already autoreduced on evacuation at 300°C. Furthermore, when the wafer was first activated under high vacuum and then reduced by H_2, the readsorption of pyridine gave an IR spectrum with no bands at 1448 cm^{-1} because the residual ruthenium cations were fully reduced. Thus, the assignment of the 1448 cm^{-1} band to Py–Ru^{n+} was confirmed, and it was concluded that it is possible to probe the existence of residual ruthenium cations within the supercages by pyridine adsorption.

As found in Section 2, the residual ruthenium cations can also be determined by the smaller probe molecule NH_3. To clarify whether the ruthenium cations all resided inside the supercages or not, the following experiment was conducted. A $Ru(NH_3)_6NaY$ wafer was first activated at 300°C under high vacuum. This treatment has been shown to provide ruthenium cations almost free of ligands (see earlier). Subsequently, the wafer was exposed to 1.0 mbar ammonia at 100°C, followed by removal of the weakly bonded ammonia by 1 h evacuation at 100°C (Fig. 11.1). After this treatment, pyridine was allowed to replace any species that occurred in accessible sites, i.e., supercages. The wafer was heated under pyridine vapor at 100°C for 2 h, then evacuated at that temperature for 1 h. It is obvious that both OH (HF) and OH (LF) groups were perturbed by pyridine molecules and pyridinium ion bands were generated (Fig. 11.2). They were similar to the bands in the spectrum of immediate pyridine

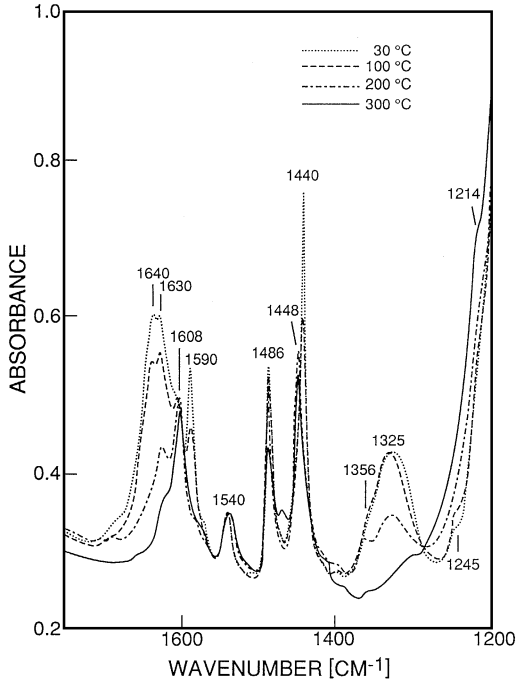

FIG. 10. *In situ* IR spectra of $Ru(NH_3)_6NaY$ on exposure to pyridine (0.5 kPa) at 30°C and subsequent heating to increasing temperatures under pyridine pressure.

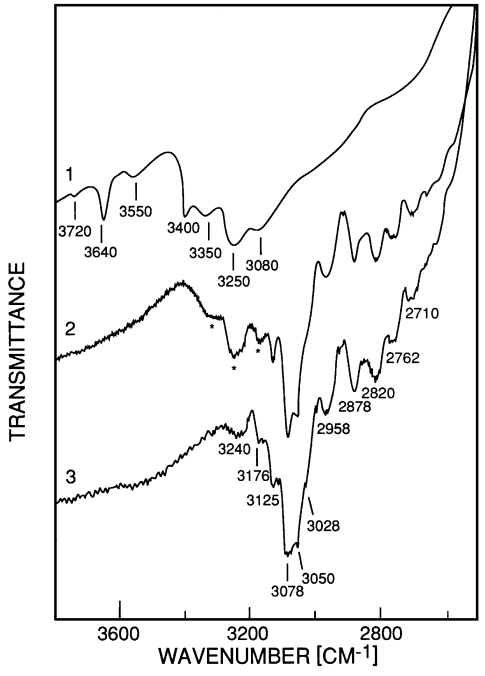

FIG. 11. IR spectra of Ru/NaHY (1) after ammonia adsorption followed by evacuation at 100°C, (2) after (1) and subsequent interaction with pyridine at 100°C, and (3) on immediate pyridine adsorption and evacuation at 100°C.

adsorption on Ru/NaHY (Fig. 11.3); however, the bands at 3350, 3250, and 3080 cm^{-1} remained and overlapped with pyridinium ion bands. Those bands were ascribed to the NH_3–Ru^{n+} species which were obviously inaccessible to pyridine molecules. Most probably, they represented the NH_3–Ru^{n+} species which were located inside the sodalite cages of Y zeolite. In conclusion, residual ruthenium cations survived vacuum pretreatment below 400°C and they could be located in both supercages and sodalite cages.

4. FTIR Measurements in the Near-Infrared Range

Near-infrared (NIR) spectroscopy can be used to investigate the overtones of OH stretching vibrations themselves as well as their combination vibrations with the in-plane and out-of-plane bending modes in zeolites (19–21). Recently, the assignment of the bands of HY zeolite in the NIR range was achieved by using the diffuse reflectance technique (22). The advantage of this technique is that the band intensities in the NIR region are much greater compared with the transmittance technique. Here, both the $Ru(NH_3)_6NaY$ and the NH_4Y zeolites were compared in the NIR range.

The NIR spectra of NH_4Y and $Ru(NH_3)_6NaY$ samples after deammoniation at 400°C are shown in Fig. 12. In the case of NH_4Y, heat treatment at 400°C removed essentially all of the H_2O and NH_3 molecules, and the NIR spectrum of the resulting HY exhibited a series of well-known bands at 7120, 6937, 4663, and 4604 cm^{-1}. They are the first overtones of the stretching vibrations of OH (HF) and OH (LF) groups and the combinations of these fundamental vibrations with the corresponding in-plane OH bending modes (22). The band at 3944 cm^{-1} is due to the combination with the out-of-plane OH bending mode.

With $Ru(NH_3)_6NaY$ zeolite, irrespective of whether it was only deammoniated at 400°C in vacuum or additionally subjected to reduction, it is interesting to note that this zeolite had almost no OH overtones and very weak combination bands in the NIR range, while the fundamental OH stretching vibrations were still very intense. To make a reasonable comparison, NIR spectra of both HY and Ru/NaHY were converted into Kubelka–Munk units, and then the relative overtone, combination, and fundamental band intensities were quantitatively estimated. It was found that the intensities of the overtone and combination bands were always 2 and 7% of those of the fundamental bands of the HY sample; however, with Ru/NaHY, the overtone and combination band intensities were only less than 0.5 and 1.0% those of the fundamental bands. These results were well reproduced. A tentative explanation may be provided by the following consideration.

Recently, it was proven by XPS that, after the above treatment, ruthenium in Y zeolite is not present as oxide particles and also not covalently bonded to the zeolite host structure (23). Formation of RuO_2 on the external crystal surface may only occur on interaction with a limited amount of lattice oxygen. Furthermore, if most of the ruthenium species were formed outside the zeolite cavities, the host composition would be similar to that of NaHY and the sample should

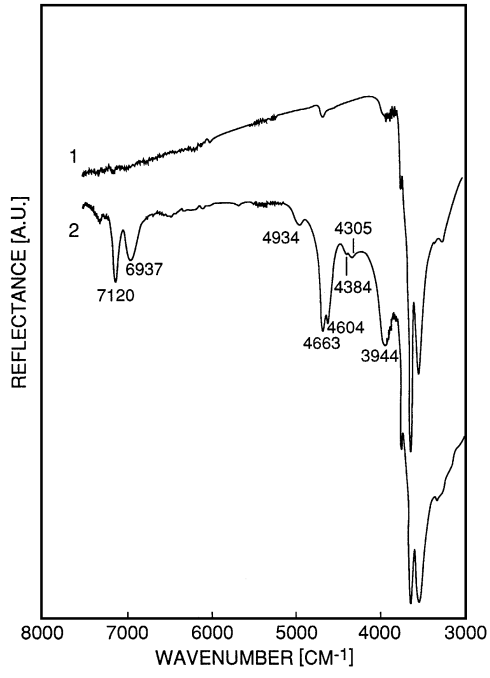

FIG. 12. NIR DRIFTS after deammoniation at 400°C of (1) $Ru(NH_3)_6NaY$ and (2) NH_4Y in high vacuum.

exhibit overtone and combination bands due to the remaining OH groups. Thus one has to assume an effect of the ruthenium-containing cationic species on the NIR spectra, even though in the case of NaHY, LaNaHY, and CaNaHY zeolites spectra with bands of OH overtones and combination modes of relatively high intensity were observed (24). According to previous results (see earlier), however, it is likely that a fraction of the ruthenium was considered to reside as Ru/O-containing clusters in the sodalite cages and/or in supercages with a high extent of dispersion and should exert a certain interaction on the Y zeolite framework. This causes, most probably, a deformation of the local geometry of the zeolite skeleton. In such circumstances, the combination of the OH fundamental vibration mode with the OH bending modes may be hindered. Thus, the NIR results would support the conclusion that ruthenium metal or metal clusters reside inside the cages of the zeolite and interact with the zeolite framework.

5. *TPD Measurements*

Temperature-programmed desorption of adsorbed ammonia is known to provide information about the distribution of the strength of acid sites; however, in the presence of ruthenium, the ammonia desorption may become more complex. The combination of TPD and mass spectrometry (TPD–MS) has the advantage of monitoring the various desorbing species simultaneously and was therefore used to investigate the ruthenium-containing zeolite. Two series of experiments were conducted: (i) TPD–MS from as-prepared NH_4Y and $Ru(NH_3)_6NaY$ zeolites (deammoniation); (ii) TPD–MS from HY and Ru/NaHY which were pretreated at 350 and 300°C *in vacuo*, respectively, and reloaded with ammonia: after deammoniation, the zeolite was cooled to 120°C, evacuated overnight, and subjected to readsorption of NH_3 (0.5 h); physically adsorbed molecules were desorbed at the same temperature for 1 h.

During temperature-programmed heating the signal intensities of $m/z = 2$ (H_2), 16 (NH_2 and O), 18 (H_2O), and 28 (N_2) were continuously monitored.

5.1. TPD–MS profiles of NH_4Y and $Ru(NH_3)_6NaY$. The TPD–MS profiles of NH_4Y and $Ru(NH_3)_6NaY$ are shown in Fig. 13. In the case of NH_4Y, both H_2O and NH_3 were released from weaker sites between 100 and 200°C. Above 200°C, NH_3 was desorbed from stronger Brønsted acid sites. The amount of H_2O desorbed at this stage was less than that in the first stage. With $Ru(NH_3)_6NaY$ it is not surprising to find the TPD profiles more complicated than those of NH_4Y. Desorption of H_2O and NH_3 predominated at temperatures below 300°C. According to the previous results (see Section 1), these H_2O and NH_3 species came mainly from the various intermediates of the decomposition of the ruthenium complex. Above 300°C, the TPD–MS profiles of N_2 species became evident. Careful inspection of the TPD features of N_2 species disclosed the fact that there

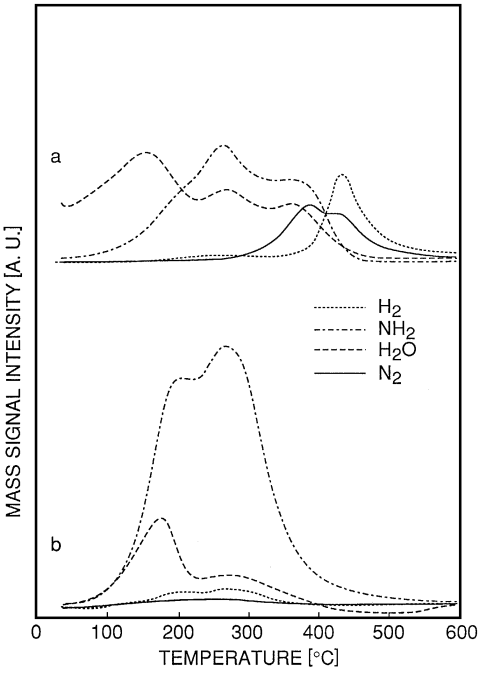

FIG. 13. TPD–MS spectra of (a) Ru/NaHY and (b) NH_4Y.

were two desorption bands, viz., at 380 and 450°C, in the TPD–MS curve of N_2. This phenomenon was more or less pronounced when using different heating rates. It can be seen from the H_2 TPD–MS curve that the H_2 generated by catalytic decomposition of NH_3 was consumed by reduction of the ruthenium cations below 400°C. This reduction accounted for the first N_2 desorption peak at 380°C. Above 400°C, the ammonia molecules were still decomposed by the reduced ruthenium metal, and both N_2 and H_2 signals could be detected.

5.2. TPD–MS profiles of NH_3–HY and NH_3–Ru/NaHY. The TPD–MS profiles of HY and Ru/NaHY, which had been reloaded with NH_3, are shown in Fig. 14. The profile of HY showed simply a broad band due to NH_3 desorption between 200 and 400°C. No H_2O was released within the temperature range of ammonia desorption; however, for the NH_3–Ru/NaHY, a different behavior can be recognized from Fig. 14. First, there were still H_2O molecules, which were mainly evolved at 320°C. Second, N_2 molecules were formed, starting at 280°C, with maxima at 330, 380, and 450°C. Finally, a pronounced H_2 peak appeared with a maximum around 450°C. Obviously, the Ru-containing sample was not completely reduced after the experiment which provided the spectra of Fig. 13a. Thus, after reloading with NH_3 and heating again, desorption of NH_3 occurred accompanied by NH_3 decomposition (on already formed Ru^0), and further reduction of Ru^{3+} (under formation of water) took place. Above 400°C, decomposition of NH_3 resulting in the evolution of N_2 and H_2 was the dominating process.

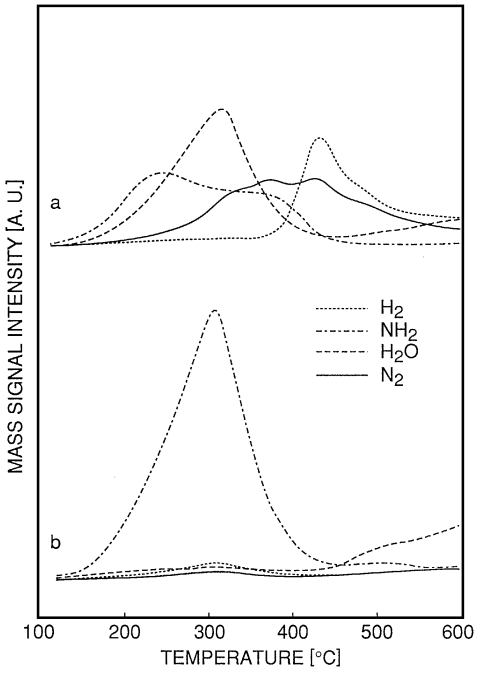

FIG. 14. TPD–MS spectra obtained with (a) Ru/NaHY and (b) HY after readsorption of NH_3.

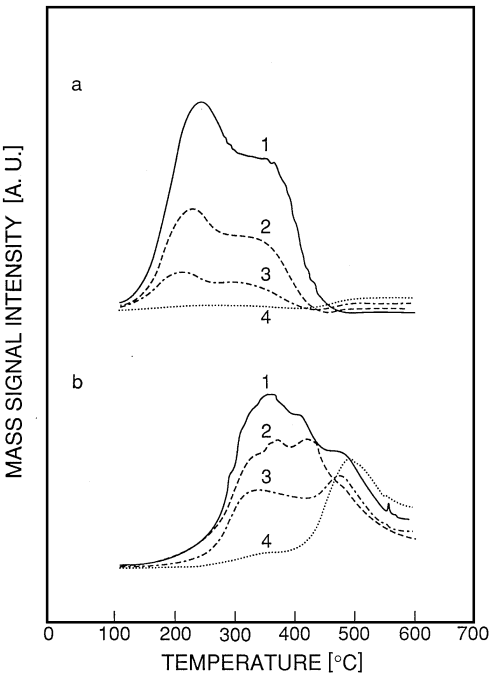

FIG. 15. TPD–MS spectra obtained with Ru/NaHY after heat treatment of $Ru(NH_3)_6NaY$ at 400°C in high vacuum and readsorption of NH_3 at 1.3 (1), 8×10^{-2} (2), 4.5×10^{-2} (3), and 6×10^{-3} mbar (4). Mass signals of (a) $m/z = 16$, NH_2, and (b) $m/z = 28$, N_2, were monitored.

The peak shapes and maximum desorption temperatures depended to a certain degree on experimental conditions; however, the TPD–MS experiments provided reproducible and reliable results when identical conditions were applied. Figure 15a suggests that only two types of acid sites existed in the Ru/NaHY zeolite. Their populations increased with increasing pressure during NH_3 loading. Clearly, at temperatures higher than 300°C, the adsorbed NH_3 molecules could be activated by ruthenium species within the zeolite cavities and underwent a decomposition into N_2 instead of simple desorption as NH_3 species (Fig. 15b). This decomposition of NH_3 was also dependent on the degree of loading with NH_3. At low coverage (NH_3 pressure of 6×10^{-3} mbar), NH_3 decomposition became evident only at high temperatures (N_2 peak at 500°C) after release of the small amount of NH_3 that was adsorbed on the strong acidic sites. Higher coverages (under NH_3 pressures of 0.045–1.30 mbar) resulted in the onset of NH_3 decomposition subsequent to the release of NH_3 from the weaker sites.

The TPD–MS profiles obtained with Ru/NaHY zeolite, which was pretreated in high vacuum at different temperatures or under reduction conditions with H_2, are shown in Fig. 16; a TPD–MS profile obtained from a NH_3–HY sample is shown for comparison (see also Fig. 14b). With the assumption of independent parallel desorption processes (8, 18), the TPD–MS profiles of NH_3 were unambiguously decomposed into three (NH_3–HY) or two (NH_3–Ru/NaHY, NH_3–reduced Ru/NaHY) different subpeaks. These computational analyses of the NH_3–TPD–MS profiles according to Ref. (7) are summarized in Table 2. The mean standard

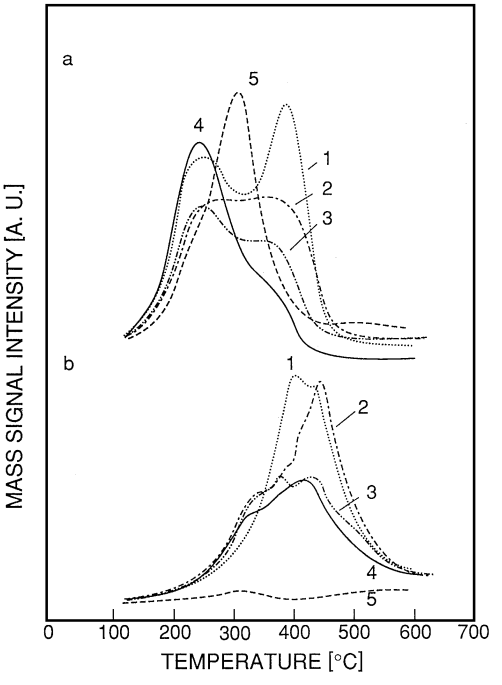

FIG. 16. TPD–MS spectra obtained after NH_3 adsorption on Ru/NaHY prepared by heat treatment of $Ru(NH_3)_6NaY$ in high vacuum at 300 (1), 350 (2), and 400°C (3); in H_2 at 400°C (4). Curve (5) shows for comparison the TPD–MS spectrum of HY after heat treatment at 400°C and loading with NH_3. Mass signals of (a) $m/z = 16$, NH_2, and (b) $m/z = 28$, N_2, were monitored.

TABLE 2

Analysis of NH_3–TPD Profiles Obtained with HY and Ru/NaHY after Various Treatments

Sample	Pretreatment	P_{NH_3} (mbar)	$\bar{E}_n$[a] (kJ/mole)			Population (%) W.A.[b]	B.A.	S.L.A
HY	400°C HV[c]	0.130	84	98	125	17	77	6
Ru/NaHY	300°C HV	0.130	89	111		56	44	
	350°C HV	0.130	91	111		60	40	
	400°C HV	0.130	88	107		65	35	
		0.080	86	104		65	35	
		0.045	83	101		65	35	
		0.006	83	99		47	53	
Ru/NaHY	400°C HV, then H_2	0.130	88	107		82	18	

[a] Most frequent activation energy of desorption from sites of type *n*, see Ref. (7).

[b] W.A., weak acid sites; B.A., Brønsted acid sites; S.L.A., strong Lewis acid sites.

[c] High vacuum.

deviations were less than 4%. In HY zeolite, the NH_3 peak at the low desorption energy [i.e., the most frequent activation energy of desorption, see Ref. (7)] of 84 kJ $mole^{-1}$ is attributable to weak acid sites, probably to residual Na^+ cations. The second and third peaks corresponding to most frequent activation energies of desorption of 98 and 125 kJ $mole^{-1}$, respectively, were assigned to Brønsted and strong Lewis acid sites, respectively. In the case of Ru/NaHY zeolites, similarly weak acid sites and Brønsted acid sites with most frequent activation energies of desorption of 83 to 91 and 99 to 111 kJ $mole^{-1}$ were found irrespective of whether the samples were treated with H_2 or not. It is unlikely that ammonia that was physically adsorbed on ruthenium metal atoms or metal clusters would have survived the 120°C desorption pretreatment before conducting the TPD experiment. Therefore, the lower desorption peak is again ascribed to desorption of NH_3 from weaker acid sites such as Na^+ and/or Ru^{n+} cations. The second peak of higher desorption energy is ascribed to NH_3 desorbing from relatively strong Brønsted acid sites; i.e., the NH_3 molecules could escape without catalytic decomposition by ruthenium metal.

From the population of those two types of sites with ammonia (see Table 2), it can be derived that the Ru/NaHY zeolite that was pretreated at 400°C in vacuum and further reduced in H_2 exhibited a higher fraction of weaker sites. Thus, NH_3 is more easily released from these samples than from Ru/NaHY, which was not treated with H_2. Moreover, the H_2-treated Ru/NaHY contained more metallic ruthenium (see Section 2). Both features rendered the H_2-treated Ru/NaHY the most efficient catalyst for NH_3 decomposition (2).

The broad bands with several maxima in the TPD profile of N_2 in Fig. 16b indicated an inhomogeneous distribution of ruthenium clusters inside the zeolite cavities. They may differ in their ability to catalyze the decomposition of NH_3 by siting in different cages or by their own structural differences (extent of aggregation or preferred growth). In any event, Ru/NaHY was shown to be catalytically active after H_2 treatment and at temperatures between 300 and 450°C.

6. *Photoelectron Spectroscopy*

To verify the chemical state of the ruthenium which cannot be detected by vibrational spectroscopy we investigated the process of thermal activation of the ammine precursor under the same conditions as in the infrared experiment with photoemission.

Figure 17 shows N 1*s* data for the sample at room temperature in UHV and after deammoniation at 400°C. The main

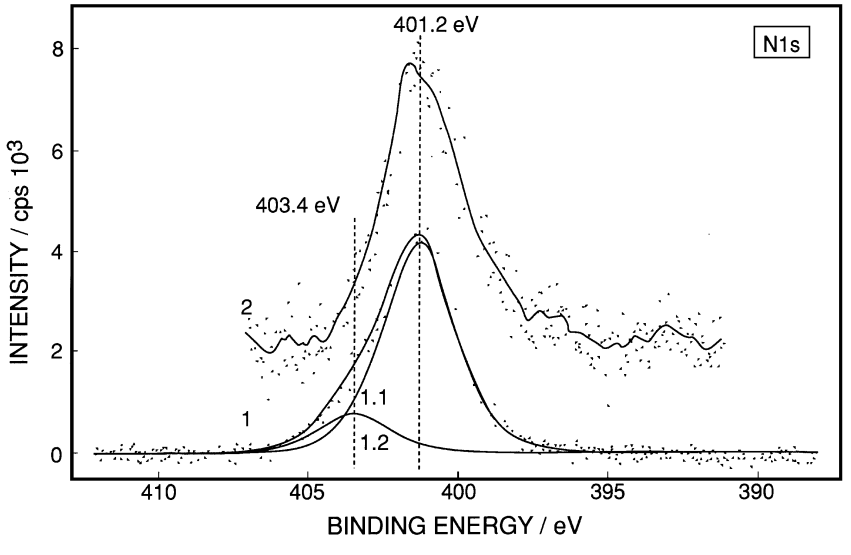

FIG. 17. XPS spectra for N 1*s* of the $Ru(NH_3)_6NaY$ zeolite evacuated at room temperature (1) and pretreated in high vacuum at 400°C (2).

peak at 401.2 eV is consistent with an ammonium ion in a nonbonding insulating environment. At room temperature there is a second component at 403.4 eV (1.2) consistent with a partially oxidized ligand such as nitroso or nitrosyl. The binding energy is distinctly lower than expected for nitrite or nitrate ligands (expected binding energy above 405 eV). The high energy contribution gradually increases with heat treatment but never dominates the spectrum, indicating that at no stage of the reaction is a major part of the ligands present in the partially oxidized state. To relate this finding to the infrared data it is important to consider the different probing depths of the two methods. Infrared data analyze the whole bulk of the sample wafer, whereas photoemission probes a thin layer of about 10 unit cells thickness. After deammoniation there is, according to the photoelectron spectrum, still a significant intensity of ammonium in the sample. The component at higher binding energy has disappeared and the total abundance of nitrogen decreased from 7.7 to 3.7 at.%. It is noted that under hydrogen reduction the nitrogen is almost completely removed, leaving less than 0.3 at.% in the sample. This finding indicates that autoreduction under the conditions chosen here was at least incomplete within the probing depth of XPS, and the material may not be the same as after activation in a more strongly reducing atmosphere. Small masses of sample release too little ammonia so that a critical threshold partial pressure of reducing species (molecular or atomic hydrogen) is not reached.

The consequence of insufficient reduction potential would be an incomplete reduction of the ruthenium and the formation of ionic species rather than metal clusters. This can be verified with ruthenium photoelectron spectra as shown in Fig. 18. The Ru 3*d* doublet and the C 1*s* level almost coincide in binding energy, giving rise to the complex features in the spectra. The narrow component with annotated binding energies represents the Ru $3d_{5/2}$ emission line. The binding energy of 283.3 eV for the precursor (1) is consistent with an ionic molecular species that is embedded in a nonbonding insulating environment. This environment affects the relaxation process of the initial photocation and gives rise to slightly more positive values for the binding energy than observed for, e.g., the bulk ruthenium compound.

Deammoniation hardly changes the binding energy but increases the linewidth of the spectrum. This is a strong indication that not a metal species but rather an ionic species with strong bonding interaction to the zeolite has been formed in the outer region of the zeolite crystallites. The strong bonding interaction gives rise to shakeup satellites and other final state effects in the spectrum resulting in a broader line.

Reduction in hydrogen (analogous to the treatment in Fig. 4) produces a mixture of small metal clusters (281.6 eV) and large ruthenium metal particles (279 eV, overcompensated charging) inside and on the external surface of the zeolite crystallites. If all metal were removed to the external surface of the zeolite crystallites and a supported metal system were the result of the activation, we would have expected a massive change in the surface composition. The ruthenium abundance of 2 at.% did not change in the deammoniation cycle and was reduced to 1.5 at.% after hydrogen reduction due to the loss of dispersion manifested in the low-binding-energy peak in Fig. 18.3.

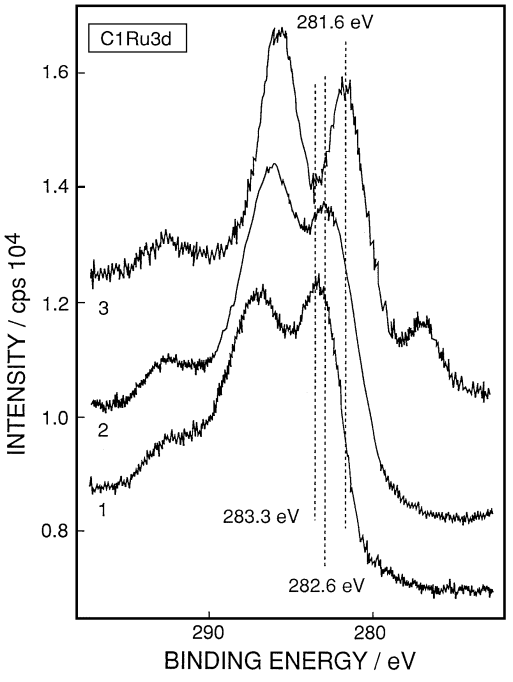

FIG. 18. XPS spectra for Ru of the $Ru(NH_3)_6NaY$ zeolite evacuated at room temperature (1); deammoniated at 400°C in high vacuum (2); and reduced in hydrogen at 400°C and 266 mbar (3).

The XPS data show that autoreduction did not result in the formation of metal clusters in the external layers but still leaves a cation-exchanged zeolite. This is not a general finding but is the consequence of the unfavorable ratio of sample volume to reactor dimensions precluding the buildup of a sufficiently strong reducing atmosphere during the process of ligand abstraction. The "naked" ruthenium has to coordinate to an oxygen function in the absence of a reducing species which would open the path to metal cluster formation. The detection of a profoundly modified zeolite matrix by vibrational data is the consequence of cation exchange and not an expression of a strong interaction between metal clusters and the zeolite matrix.

CONCLUSIONS

All the data obtained with $Ru(NH_3)_6NaY$ indicate that autoreduction and reduction by hydrogen lead to significantly different products. Autoreduction under different experimental conditions (IR, TPD, and XPS experiments)

always resulted in incomplete reduction, whereas reduction in hydrogen was complete. Comparison between the results of bulk-sensitive IR and TPD and surface-sensitive XPS showed that metallic Ru^0 particles were formed only in the interior of the zeolite crystallites. The identification of ionic ruthenium besides metallic ruthenium is in contrast to earlier XPS observations (2, 3); XPS alone is not able to detect the coexistence of two valence states of Ru.

The present study has shown that (i) on heat treatment of $Ru(NH_3)_6NaY$ in high vacuum, various intermediates of decomposition can be identified via *in situ* IR spectroscopy, in particular complexes with nitrosyl ligands; (ii) OH groups formed due to the decomposition of $Ru(NH_3)_6NaY$ are affected by the presence of ruthenium; (iii) the ruthenium ammine complex can be recovered to some extent via ammonia readsorption; (iv) siting of ruthenium species in both the supercages and sodalite cages can be determined by IR using NH_3 and pyridine as probes; and (v) NIR measurements seem to indicate a strong effect of ruthenium-containing species inside the zeolite structure leading to a lack of combination bands of the OH stretch and bending modes. TPD–MS of ammonia from variously treated $Ru(NH_3)_6NaY$ (as-prepared, decomposed in high vacuum, reduced in H_2) provides information about the acidic properties of the materials and the presence of part of the ruthenium as metal particles.

ACKNOWLEDGMENTS

S.-P.S. acknowledges grants from the Science Foundation of the Republic of China and the Max Planck Society. The authors are indebted to Mrs. Ute Wild, Mrs. Erika Popovic, and Mr. Walter Wachsmann for valuable experimental assistance. They thank the referees for valuable suggestions, inter alia for the alternative explanation of the NO frequency shifts.

REFERENCES

1. Tennison, S. R., *in* "Catalytic Ammonia Synthesis," (J. R. Jennings, Ed.), p. 303, Plenum, New York, 1991.
2. Mahdi, W., Sauerlandt, U., Wellenbüscher, J., Schütze, J., Muhler, M., Ertl, G., and Schlögl, R., *Catal. Lett.* **14**, 339 (1992).
3. Wellenbüscher, J., Rosowski, F., Klengler, U., Muhler, M., Ertl, G., Guntow, U., and Schlögl, R., "Zeolites and Related Microporous Materials: State of the Art 1994" (J. Weitkamp, H. G. Karge, H. Pfeifer, and W. Hölderich, Eds.), Part A, p. 941. Elsevier, Amsterdam, 1994.
4. Cisneros, M. D., and Lunsford, J. H., *J. Catal.* **141**, 191 (1993).
5. Karge, H. G., and Klose, K., *Z. Phys. Chem. NF* **83**, 92 (1973).
6. Karge, H. G., Abke, W., Boldingh, E. P., and Łaniecki, M., *in* "Proceedings, 9th Iberoamerican Symposium on Catalysis, Lisbon, 1989" (M. F. Portela, Ed.), p. 582. Jorge Fernandes, 1984.
7. Kazansky, V. B., Borovkov, V. Yu., and Karge, H. G., *J. Chem. Soc. Faraday Trans.*, in press.
8. Karge, H. G., and Dondur, V., *J. Phys. Chem.* **94**, 765 (1990).
9. Verdonck, J. J., Schoonheydt, R. A., and Jacobs, P. A., *J. Phys. Chem.* **85**, 2393 (1981).
10. Madhusudhan, C. P., Patil, M. D., and Good, M. L., *Inorg. Chem.* **8**, 2384 (1979).
11. Pearce, J. R., Gustafson, B. L., and Lunsford, J. H., *Inorg. Chem.* **20**, 2957 (1981).
12. Goldwasser, M., Dutel, J. F., and Naccache, C., *Zeolites* **9**, 54 (1989).
13. Johnson, B. F. G., and McCleverty, J. A., *Prog. Inorg. Chem.* **7**, 277 (in particular, p. 339) (1996).
14. Hirschler, A. E., *J. Catal.* **2**, 428 (1963).
15. Plank, C. J., *in* "Proceedings 3rd International Congress on Catalysis, Amsterdam, 1964" (W. M. H. Sachtler, G. C. A. Schuit, and P. Zwietering, Eds.), Vol. 1, p. 727. North-Holland, Amsterdam, 1965.
16. Davydov, A. A., *in* "Infrared Spectroscopy of Adsorbed Species on the Surface of Transition Metal Oxides" (C. H. Rochester, Ed.), p. 27, Wiley, New York, 1990.
17. Nakamoto, K., "Infrared Spectra of Inorganic and Coordination Compounds," p. 143. Wiley, New York, 1963.
18. Pearce, J. R., Mortier, W. J., and Uytterhoeven, J. B., *J. Chem. Soc. Faraday Trans. 1* **75**, 1395 (1979).
19. Staudte, B., Hunger, M., and Nimz, M., *Zeolites* **11**, 837 (1991).
20. Kustov, L. M., Borovkov, V. Yu., and Kazansky, V. B., *J. Catal.* **72**, 149 (1981).
21. Jacobs, W. P. J. H., Jobic, H., van Wolput, J. H. M. C., and van Santen, R. A., *Zeolites* **12**, 315 (1992).
22. Beck, K., Pfeifer, H., and Staudte, B., *Microporous Mater.* **2**, 1 (1993).
23. Wellenbüscher, J., Sauerland, U., Mahdi, W., Ertl, G., and Schlögl, R., *Surf. Interface Anal.* **18**, 650 (1992).
24. Sheu, S.-P., Karge, H. G., and Schlögl, R., unpublished results.